1

Redox Equilibria: From Basic Concepts to the Magmatic Realm

Roberto Moretti[1,2] and Daniel R. Neuville[1]

ABSTRACT

The basic aspects of redox geochemistry are reviewed to provide a useful compendium of the redox connection between the aqueous-hydrothermal and igneous realms of Earth. The redox description of a system is intimately coupled to the knowledge of acid-base properties of the solvent in which redox exchanges take place. For magmas, and then silicate melts, approaches reporting the redox state were so far cantered around the sole concept of oxygen fugacity, fO_2. Mastering the concept of fO_2 in experimental and observational petrology was the key to constrain the processes behind the very large range of relative oxygen fugacity observed on Earth. Although current descriptions of silicate melts and magma thermodynamic properties are mainly based on oxides or mineral-like molecular components, disregarding the actual melt reactivity poses many limits in our understanding of the true chemical exchanges involving oxygen, iron and the other redox-sensitive elements. Because silicate melts, unlike aqueous solutions, lack of a full acid-base description, compositional dependencies are solved by means of empirical treatments based on oxides and their combinations. However, these can bias the interpretation of redox exchanges recorded in analyzed samples and used to identify the several processes (e.g., batch or fractional crystallization, elemental recycling, degassing, deep fluid infiltration) which characterize magma evolution and its geodynamic environment. This short compendium aims at stimulating the quest for a comprehensive and unifying picture of the acid-base and redox properties of melts from which we could extrinsic its reactivity in way similar to aqueous solutions and molten salts.

1.1. GENERAL ASPECTS AND RATIONALE

1.1.1. Oxidation Number, Electron Transfer, and Half-Reactions

Oxidation-reduction (redox) geochemistry studies those natural reactions occurring on Earth in which the transfer of electrons determines a change in the oxidation number of participating chemical species. Oxidation state (or oxidation number) measures the degree of oxidation of an atom in a substance and it is the (hypothetical) charge of an atom if all bonds to atoms of different elements were 100% ionic, with no covalent bond fraction. The oxidation state of an atom is indicated with Roman numerals, whereas Arabic numbers are used for the charge on compound (e.g., in SiO_4^{4-}, silicon has oxidation number IV and oxygen has –II, whereas 4– is the formal charge of the whole silicate ion). Charge and oxidation number are the same for monoatomic ions. The oxidation number can be positive, negative, or zero, and it can have a

[1]*Université de Paris, Institut de Physique du Globe de Paris, Paris, France*

[2]*Observatoire Volcanologique et Sismologique de Guadeloupe, Institut de Physique du Globe de Paris, Gourbeyre, France*

Magma Redox Geochemistry, Geophysical Monograph 266, First Edition.
Edited by Roberto Moretti and Daniel R. Neuville.

DOI: 10.1002/9781119473206.ch1

fractional value as well, and although very similar, it does not correspond to valency, which is an atom property and represents the number of bonds the atom needs to become stable, i.e., to complete either duplet or octet rule.

Many redox reactions are familiar to us, such as fire and combustion, rusting, and dissolution of metals. Transition metals and main group elements (e.g., N, halogens, O, S, C) have multiple oxidation states and important redox chemistry, which affect element distribution within the geochemical shells on Earth but also through the boundaries between such shells (e.g., Moretti et al., 2020a). For instance, it is the redox state of metals and ligands that complex them, which then determines (i) their "unlocking" from pristine reservoirs (e.g. minerals in which they occur at trace level); (ii) their mobility on Earth through carriers such as magma, water, or vapor; and eventually (iii) their accumulation and precipitations in new phases making up ore deposits.

Redox reactions involve a coupled transfer of electrons, so for any oxidation (loss of electrons) a reciprocal reduction (gain of electrons) occurs. Moreover, redox reactions naturally occurring on Earth involve a net chemical change that can be described not only via the exchange of electrons between ions or their complexes, but also of oxygen and/or hydrogen atoms and compounds that these can form (e.g., Cicconi et al., 2020a and references therein). Here are some examples:

$$2Fe_{(s)} + O_{2(g)} \Leftrightarrow 2FeO_{(s)} \quad (1.1)$$

$$2FeO_{(m)} + H_2O_{(g)} \Leftrightarrow Fe_2O_{3(m)} + H_{2(g)} \quad (1.2)$$

$$Fe^{3+}{}_{(aq)} + \tfrac{1}{2}H_{2(g)} \Leftrightarrow Fe^{2+}{}_{(aq)} + H^{+}{}_{(aq)} \quad (1.3)$$

$$4Fe^{2+}{}_{(aq)} + O_{2(g)} + 4H^{+}{}_{(aq)} \Leftrightarrow 4Fe^{3+}{}_{(aq)} + 2H_2O_{(aq)} \quad (1.4)$$

$$SO_{2(g)} + 3H_{2(g)} \Leftrightarrow H_2S_{(g)} + 2H_2O_{(g)} \quad (1.5)$$

In which the subscripts *s*, *m, aq*, and *g* refer to solid, melt, aqueous, and gas (including supercritical fluids) phases, respectively. In the five examples above, $O_{2(g)}$, $H_2O_{(g)}$, $Fe^{3+}{}_{(aq)}$, $O_{2(g)}$ and $SO_{2(g)}$ are oxidizing agents, whereas $Fe_{(s)}$, $FeO_{(l)}$, $H_{2(g)}$, $Fe^{2+}{}_{(aq)}$ are the reducing agents.

The word oxidation was introduced by Antoine Lavoisier (1777) and indicates the chemical mechanisms in which oxygen is consumed and added to a compound. The parallel mechanism in which some other compounds loose oxygen was called reduction. The oxidation number of reaction components in Reactions 1.1 to 1.5 shows that some elements have a greater affinity for electrons than others and that oxygen tends to appear with oxidation number –II in its compounds (including the O^{2-} species in its ionic compounds). In contrast, hydrogen tends to appear with oxidation number I. Besides, hydrogen and oxygen atoms and their compounds in reaction are related to ligands making up the most important matrixes on Earth, such as aqueous solutions (including highly concentrated saline solution), supercritical fluids and gases, silicate melts or oxide, and silicate minerals making up rocks. Except for rocks, these matrixes are also important transport agents and thus redox carriers within Earth geochemical reservoirs and throughout their boundaries. Therefore, nearly all redox exchanges on Earth are related to chemical transfers involving hydrogen- and/or oxygen-based half-reactions such as (Cicconi et al., 2020a,b):

$$O_2 + 4e^- \Leftrightarrow 2O^{2-} \quad (1.6)$$

$$2H^+ + 2e^- \Leftrightarrow H_2 \quad (1.7)$$

that we will call henceforth oxygen and hydrogen electrodes (e.g., Cicconi et al., 2020a; Moretti, 2020) and in which the electron exchange is made explicit. For example, Reaction 1.1 can be written as the sum of Reaction 1.6 and:

$$2Fe^0 \Leftrightarrow 2Fe^{2+} + 4e^- \quad (1.8)$$

plus the formation of FeO oxides from its ions,

$$2Fe^{2+} + 2O^{2-} \Leftrightarrow 2FeO \quad (1.9)$$

in which oxidation numbers and then formal charges of involved atoms do not vary.

In ore geochemistry, but also in metallurgical practice, a special mention must be made to redox mechanisms involving chalcophile elements and sulfide. Most often, relevant equilibria are written without the involvement of the medium in which they actually occur. Pyrite formation can result from the hydrothermal alteration of igneous pyrrhotite, but their equilibrium can be simply written in the sole Fe–S system as (Barton, 1970):

$$2FeS + S_2 \Leftrightarrow 2FeS_2 \quad (1.10)$$

In the Fe–S system, pyrite is not at the liquidus (pyrite does not melt), but as a conceptual exercise we can still relate its formation to the occurrence of the following fictitious half-reactions in the solid phase involving sulfide and polysulfide anions:

$$S_{2(g)} + 2e^- \Leftrightarrow 2S^{2-} \quad (1.11)$$

$$S_2{}^{2-} + 2e^- \Leftrightarrow 2S^{2-} \quad (1.12)$$

and their combination with iron, which appears in its cationic form Fe^{2+} in both sides of Reaction 1.10. In the

liquid state, melts in which sulfide is the main or the sole anionic ligand are very scarcely represented on Earth and segregate from reducing sulfur oversaturated magmatic silicate melts (e.g., Li and Ripley, 2013 and references therein). Instead, sulfide melts are of interest in extractive metallurgy (e.g., Sokhanwaran et al., 2016).

1.1.2. The Redox Potential in Solutions and the Ligand Role

In redox reactions a potential difference drives the transfer electrons from an anode (negative electrode) to a cathode (positive electrode): oxidation occurs at the anode and reduction occurs at the cathode. Reactions are spontaneous in the direction of $\Delta G < 0$, which is also the direction in which the potential (defined as $E_{cathode} - E_{anode}$) is positive. In a redox reaction the anode is then the half-reaction written with electrons on the right and the cathode is the half-reaction with electrons appearing on the left side.

The electric work done by a spontaneous redox reaction, like in a galvanic cell ($E > 0$), is the (measurable) electromotive force of the reacting systems and equals the Gibbs free energy change (e.g. Ottonello, 1997) via the Nernst equation:

$$-nFE = \Delta G = \Delta G^0 + RT\ln\prod a_i = -nFE^0$$

$$+ 2.303RT\log\prod a_i = -nFE^0 + 2.303RT\log Q_i \quad (1.13)$$

with a_i the activity of the i^{th} component participating in the redox exchange, F as the Faraday constant (96,485 Coulomb per mole), n the number of transferred electrons, and Q the activity product. In writing redox reactions, complete electrolytes are often used because the activity coefficients are measured without extra thermodynamic assumptions, but Equation 1.13 is normally used for reactions based on individual ions. To establish a potential scale for half-reactions, we keep using the convention that electrons are reported on the left-hand side of the reaction, that is, in the sense of reduction. The potentials of half-reactions can be added and subtracted, like free energies, to give an overall value for the reaction. It is also worth noting that by convention, it was decided to use a hydrogen-electrode-scale electric potential, by setting $E^0 = 0.0$ V for reaction 1.7 with the constituents in their standard state (e.g., Casey, 2017). This arbitrary decision implies that (i) the Gibbs energy for $H^+_{(aq)}$, the electron (e^-), and $H_{2(g)}$ are all 0.0 kJ/mol, and (ii) potential difference of reactions involving the hydrogen electrode (Reaction 1.7) are given by the other half-reaction completing the redox exchange.

The electrode potential values (E^0) hold at standard conditions: by definition, standard conditions mean that any dissolved species have concentrations of 1 m, any gaseous species have partial pressures of 1 bar, and the system is 25°C. Standard potentials represent the case where no current flows and the electrode reaction is reversible. Measuring a voltage is an indication that the system is out of equilibrium. Nernstian processes are characterized by fast electron transfer and are rate-limited by the diffusion of the electron-active species into the electrolyte. The system then spontaneously approaches equilibrium because negative and positive charged species can flow in opposite directions. At equilibrium, the voltage drops to zero and the current stops, like in dead batteries. The magnitude of the cell potential, $E^0 = E^0_{cathode} - E^0_{anode}$, may be viewed as the driving force for current flow in the circuit.

The hydrogen-electrode scale electric potential so defined, E (also indicated as E_h in aqueous solutions), is a measure of the oxidation state of a system at equilibrium relative to a hydrogen electrode. E is not a constant (for given T and P) but depends on the system composition via activities of ions entering a half redox reaction. When coupled to a compositional parameter of the system related to the activity of the ligand making up the solvent of interest, such as a_H+ for aqueous solutions, E can be used to establish a kind of phase diagram that shows which species (dissolved ion species, gases, or solids) will predominate among a chosen set in the system of interest (a solution) for a given temperature.

To easily understand all this, we can look at the reaction leading to the formation of liquid water:

$$2H_{2(g)} + O_{2(g)} \Leftrightarrow 2H_2O_{(aq)} \quad (1.14)$$

which is given by the sum of Reaction 1.7 (H^+/H_2 redox couple: the anode) and the following half-reaction (the cathode):

$$O_{2(g)} + 4H^+_{(aq)} + 4e^- \Leftrightarrow 2H_2O_{(aq)} \quad (1.15)$$

which is governed by the O_2/H_2O redox couple. The presence of protons in both Reactions 1.7 and 1.15 shows that the overall Reaction 1.14 is defined for acidic conditions ($pH < 7$). For neutral or basic conditions ($pH \geq 7$), Reaction 1.14 can be obtained from the following two half-reactions for H_2O/H_2 and O_2/OH^- couples, respectively:

$$2H_2O_{(aq)} + 2e^- \Leftrightarrow H_{2(g)} + 2OH^- \quad (1.16)$$

$$O_{2(g)} + 2H_2O + 4e^- \Leftrightarrow 4OH^- \quad (1.17)$$

Let us now deal with Reactions 1.7 and 1.15 occurring in the acidic medium (see, for example, Ottonello, 1997). The standard potential of Reaction 1.15 is $E^0_{16} = 1.228$ V and refers to a standard state of water in equilibrium at

T = 25°C and P = 1 bar with an atmosphere of pure O_2. From Equation 1.13 we obtain:

$$E_{15} = 1.228 + 0.0591 \log aH^+ + 0.0148 \log aO_2$$
$$= 1.228 - 0.0591 pH + 0.0148 \log fO_2 \quad (1.18)$$

where a and f denote activity and fugacity, respectively, $pH = -\log a_H+$ and it is considered that $aO_2 = fO_2/fO_2^0$ with $fO_2^0 = 1$ bar.

Similarly, the redox potential related to Reaction 1.7 is then:

$$E_7 = -0.0591 pH - 0.0295 \log fH_2 \quad (1.19)$$

Equations 1.18 and 1.19, which can also be derived for Reactions 1.16 and 1.17, can be used to trace E-pH diagrams (also called Pourbaix or predominance diagrams; Casey, 2017) limiting the stability field of water (Figure 1.1) and of any other systems in which E-pH relationships can be established from the reactions of intervening species (Figure 1.2). E-pH diagrams are most used for understanding the geochemical formation, corrosion and passivation, leaching and metal recovery, water treatment precipitation, and adsorption.

For the set of species of interest, E-pH diagrams show boundaries that are given by:

1. lines of negative slope that limit the stability field of water (Equations 1.18 and 1.19) or related to solid–solid phase changes in which paired electron–proton exchanges occur because the ligand (water) participates in reaction, such as in the case of the hematite–magnetite boundary in Figure 1.2:

$$3Fe_2O_3 + 2H^+ + 2e^- \Leftrightarrow 2Fe_3O_4 + H_2O \quad (1.20)$$

Note that boundary slope is negative because protons and electrons appear on the same side of reaction. The protons/electrons ratio determines the slope value.

2. (rare) pH-dependent lines of positive slopes, and associated with electron–proton exchanges involving, for example, reduction of dissolved cations to the oxide with a lower oxidation number, e.g.

$$2Cu^{2+} + H_2O_{(aq)} + 2e^- \Leftrightarrow Cu_2O_{(s)} + 2H^+ \quad (1.21)$$

Boundary slope is positive because protons and electons appear on different sides of reaction.

3. horizontal lines (pure electron exchange), such as in case of half-reaction

$$Fe^{3+} + e^- \Leftrightarrow Fe^{2+} \quad (1.22)$$

which participates with half-reaction 1.7 in giving Reaction 1.3 and does not involve explicitly the water solvent.

4. vertical lines, representing no change of oxidation state but only acid–base reactions (a sole exchange of protons for aqueous solutions), such as

$$2Fe^{3+} + 3H_2O \Leftrightarrow Fe_2O_{3(s)} + 6H^+ \quad (1.23)$$

with the boundary plotted at the pH value for which $Q_{23} = K_{23}$ with $aFe_2O_{3(s)} = (aFe^{3+})^2 = 1$ (and also $aH_2O = 1$).

We now see that Reactions 1.3 and 1.4 are both related to half-reaction 1.22, but they refer to different redox conditions and then have different meanings. In Reaction 1.3 water is the oxidizing agent in acidic conditions, whereas it is the reducing agent in Reaction 1.4 (Appelo and

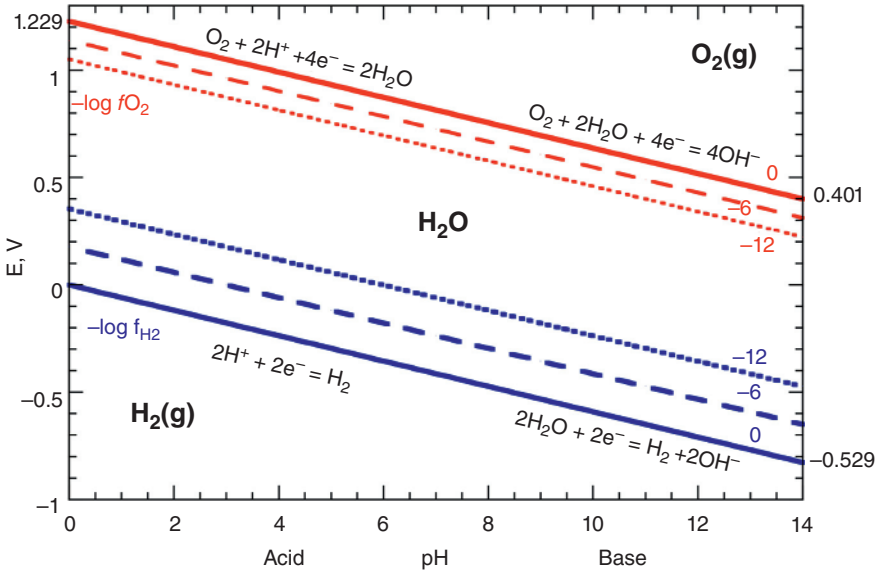

Figure 1.1 E-pH diagram reporting the stability of water at T = 25°C and P = 1 bar for different partial pressure of H_2 and O_2 (log-values).

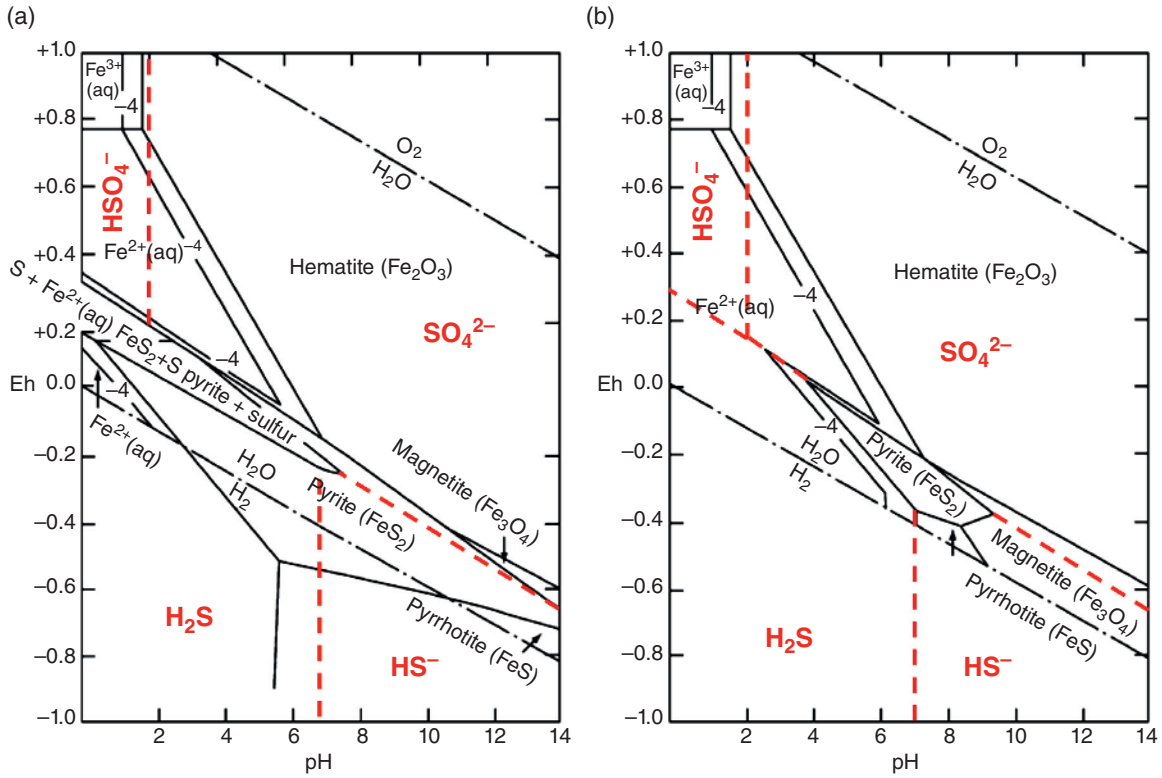

Figure 1.2 The E-pH (Pourbaix) diagram for the Fe-S-H_2O system at 25°C at 1 bar total pressure and for total dissolved sulfur activities of 0.1 (panel a) and 10^{-6} (panel b). Superimposed are the stability fields for H_2S, HS^-, HSO_4^{2-} and SO_4^{2-} dissolved species (red lines, traced from data in Biernat and Robins, 1969). Note how the field of stability of pyrite, FeS_2, shrinks and that of magnetite, Fe_3O_4, expands with decreasing total sulfur activity. Modifed from Vaughan (2005).

Postma, 1996), which represents a regulating mechanism of O_2, probably the oxidative alteration of rocks containing Fe^{2+}, in particular at oceanic ridges.

Basically, E-pH diagrams demonstrate that breaking of a redox reaction into half-reactions is one of the most powerful ideas in redox chemistry, which allows relating the electron transfer to the charge transfer associated with the speciation state and the acid–base behavior of the solvent. Superimposing E-pH diagrams allows a fast recognition of the existing chemical mechanism occurring in an electrolyte medium. For example, Figure 1.2 on the Fe-H-O-S system can be seen as the result of the superposition of stability diagrams for H-O-S and Fe-O-H system. The resulting diagram in Figure 1.2 shows that the pyrite–magnetite boundary has a negative slope due to half-reaction:

$$Fe_3O_{4(s)} + 6SO_4{}^{2-}{}_{(aq)} + 56H^+{}_{(aq)} + 44e^- \Leftrightarrow 3FeS_{2(s)} + 28H_2O_{(aq)} \quad (1.24)$$

but also a positive slope well visible in Figure 1.2b due to sulfur reduction and dissolution in water as HS^-:

$$3FeS_{2(s)} + 4H_2O_{(aq)} + 4e^- \Leftrightarrow Fe_3O_{4(s)} + 6HS^-{}_{(aq)} + 2H^+{}_{(aq)} \quad (1.25)$$

Reaction 1.25 implies of course a positive slope, because H^+ appears on the right side and electrons on the left. We can also appreciate the reduction of sulfur from pyrite to pyrrhotite at pH > 7:

$$FeS_{2(s)} + H^+ + 2e^- \Leftrightarrow FeS_{(s)} + HS^-{}_{(aq)} \quad (1.26)$$

which has a negative slope of –0.0295pH because the number of exchanged electrons is double than protons.

These concepts can then be transferred to other solvents in which ligand–metal exchanges lead to a different speciation state and are governed by a different notion of basicity, i.e. oxobasicity, such that (see Moretti, 2020 and references therein):

$$\text{Base} \Leftrightarrow \text{Acid} + O^{2-} \quad (1.27)$$

which can be also related to redox exchanges via the *normal oxygen electrode* (Equation 1.6), in the same way the normal hydrogen electrode (Reaction 1.7) can be put in relation with the Bronsted-Lowry definition of acid–base behaviour in aqueous solutions (see Moretti, 2020):

$$\text{Base} + H^+ \Leftrightarrow \text{Acid} \quad (1.28)$$

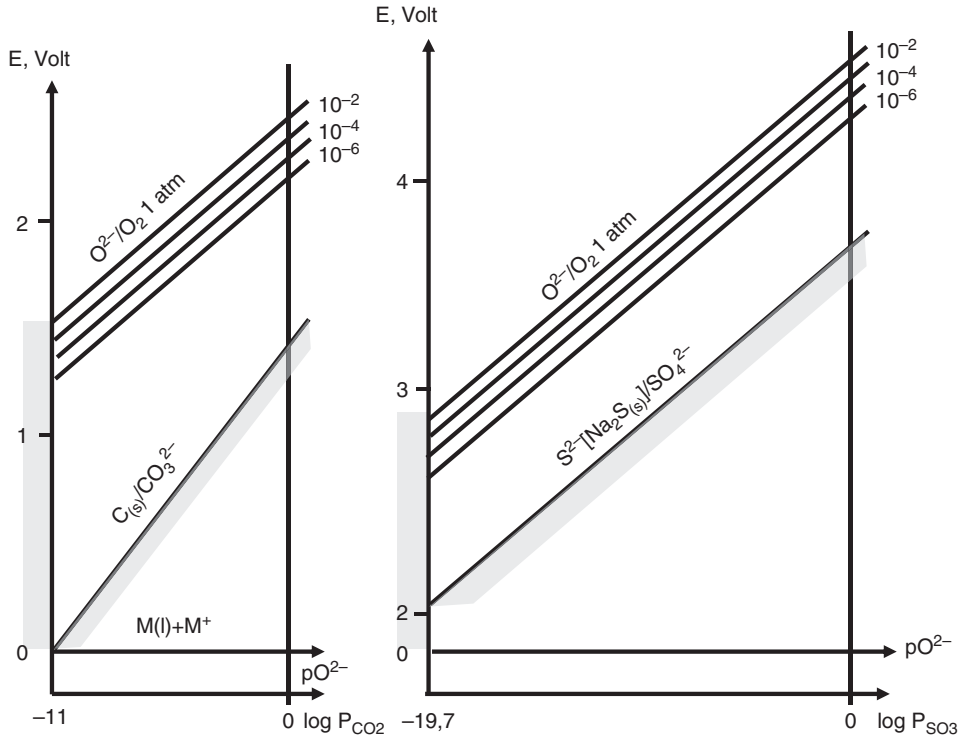

Figure 1.3 Limit of equilibrium potential-pO^{2-} graphs in molten alkali carbonates and sulfates, at 600°C (modified from Trémillon, 1974).

It is then possible to define $pO^{2-} = -\log aO^{2-}$ and introduce E-pO^{2-} diagrams, in which acid species will be located at high pO^{2-} values. These diagrams were first introduced by Littlewood (1962) to present the electrochemical behaviour of molten salt systems and provide an understanding of the stability fields of the different forms taken by metals in these systems. Reference potential for molten salt is chosen either from anion or from cation, but anion, making up the ligand, is normally selected because there may be several different cations in the system.

For molten solvent diagrams, such as carbonate and sulfate melts, the stability area of the bath depends on the salt itself and can be seen by using as examples oxyanion solvents (Figure 1.3). Limitations on the pO^{2-} scale of oxoacidity (Reaction 1.27) are given by the values of the Gibbs free energy of the formation reactions of alkali carbonates or sulfates at the liquid state, which depends on temperature as well as on pressure. On the basic side (low pO^{2-} side) the limit is imposed by the solubility threshold of the generic $M^{\nu+}O_{\nu/2}$ oxide in the electrolyte medium, i.e., $pO^{2-}\text{min} \approx M^{\nu+}O_{\nu/2}$ solubility, whereas on the acidic side the limit is imposed by P_{CO2} or $P_{SO3} = 1$ bar. For example, it is 11 units in the case of the ternary eutectic Li_2CO_3+Na_2CO_3+K_2CO_3 at 600°C and 19.7 units in the case of the ternary eutectic Li_2SO_4 + Na_2SO_4 + K_2SO_4 at the same temperature (Trémillon 1974; Figure 1.3).

The upper stability limit is related to the $O^{-II}/O_{2(g)}$ redox system (Reaction 1.6), i.e., to the oxidation of CO_3^{2-} and SO_4^{2-} anions:

$$CO_3^{2-} \Leftrightarrow \tfrac{1}{2}O_{2(g)} + CO_{2(g)} + 2e^- \qquad (1.29)$$

$$2SO_4^{2-} \Leftrightarrow \tfrac{1}{2}O_{2(g)} + S_2O_7^{2-} + 2e^- \qquad (1.30)$$

which results from acid–base exchanges of the type:

$$CO_3^{2-} \Leftrightarrow CO_{2(g)} + O^{2-} \qquad (1.31)$$

$$2SO_4^{2-} \Leftrightarrow S_2O_7^{2-} + O^{2-} \qquad (1.32)$$

coupled to half-reaction 1.6.

Both Reactions 1.29 and 1.30 yield the E-pO^{2-} relationship:

$$E = E^0_{O_2} + \frac{2.3RT}{4F}\log P_{O_2} + \frac{2.3RT}{2F}pO^{2-} \qquad (1.33)$$

The lower stability limit of the solvent can be given by either the reduction of alkaline cation in the corresponding metal:

$$M^{\nu+} + \nu e^- \Leftrightarrow M_{(l)} \qquad (1.34)$$

whose potential is independent of pO^{2-}, or the reduction of CO_3^{2-} and SO_4^{2-} anions given by:

$$CO_3^{2-} + 4e^- \Leftrightarrow C_{(s)} + 3O^{2-} \qquad (1.35)$$

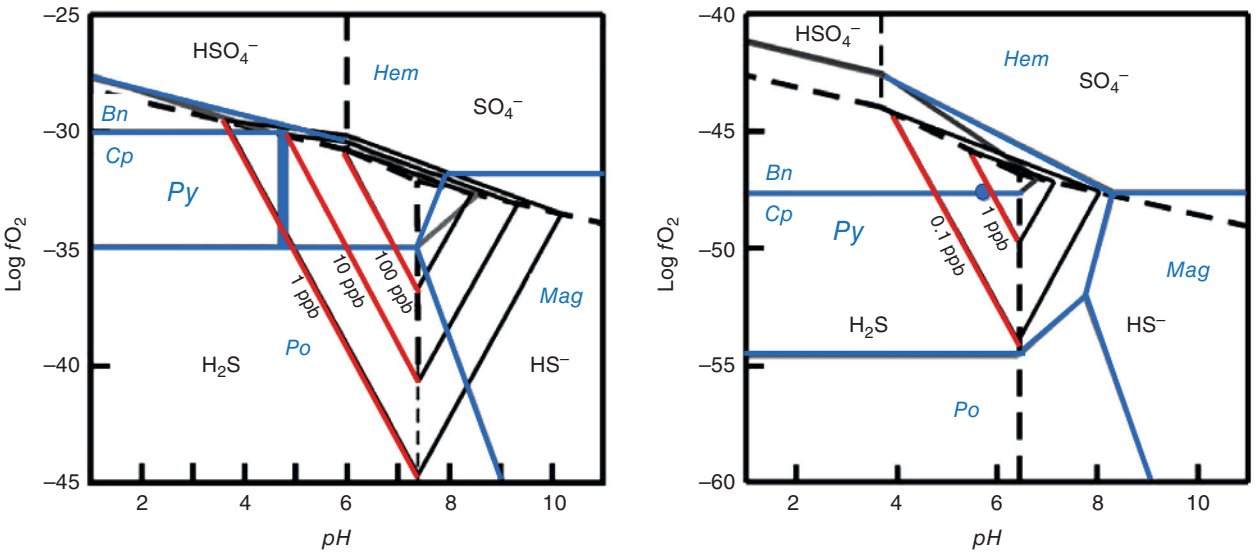

Figure 1.4 Log fO_2 - Ph diagrams for 290°C (left panel) and 145°C (right panel) at saturated vapor pressure, showing predominance fields for aqueous sulfur species (dashed lines), stability fields for Fe–O–S minerals and bornite–chalcopyrite (solid grey lines). The solubility contours (left panel: 1, 10, 100 ppm; right panel: 0.1, 1 ppm) are for gold in the form $Au(HS)_2^-$. Modified from Raymond et al. (2005).

$$SO_4^{2-} + 8e^- \Leftrightarrow S^{2-} + 4O^{2-} \quad (1.36)$$

and to which the following E-pO^{2-} relationships correspond (CO_3^{2-} and SO_4^{2-} anions having unitary activity):

$$E = E^0_{C/CO_3^{2-}} + \frac{3}{4}\cdot\frac{2.3RT}{F}pO^{2-} \quad (1.37)$$

$$E = E^0_{S^{2-}/SO_4^{2-}} - \frac{2.3RT}{8F}\log\left[S^{2-}\right] + \frac{2.3RT}{2F}pO^{2-} \quad (1.38)$$

Figure 1.3 shows the results on carbonate and sulfate melts (modified from Trémillon, 1974, and references therein). The utilizable regions appear as quadrilaterals on the E-pO^2 graph. If in sulfates, the region is a parallelogram similar to the E-pH region in aqueous solution, the theoretical range of potential in molten carbonates appears more restricted in an oxoacidic medium than in an oxobasic medium, because the lower limit varies versus pO^{2-} with a slope greater than that of the upper limit (Trémillon, 1974).

Silicate melts have been so far an underestimated electrolytic medium acting as a solvent for oxides. This is mainly because E-pO^{2-} diagrams cannot be based on predictive thermodynamics and physical chemistry assessments such as the dilute electrolyte concept and its developments in the case of previous solvents, aqueous solutions particularly (Allanore, 2015). In silicate melts, and more generally molten oxides, oxygen *toutcourt* cannot be identified as the solvent, despite its abundance. Silicate melts are in fact a high-temperature highly interconnected (polymerized) matrix in which solvation units cannot be easily defined and both ionic and covalent bonds rule the reactive entities that make up the melt network. Because of this, some approaches have been formalized in terms of the Lewis acid–base definition (network formers and their oxides, such as SiO_2 and Al_2O_3 are acids; network modifiers and their oxides such as MgO, CaO, Na_2O are bases) by using electronegativity and optical basicity that allow distinguishing and calculating three types of oxygen (bridging, non-bridging, and so-called free oxygen) whose mixing determines the polymerization and the thermodynamic properties of the melt mixture as a function of composition (Toop and Samis, 1962a,b; Allanore, 2013, 2015 and references therein; Moretti, 2020 and references therein). Nevertheless, silicate melts still lack a fully developed acid–base framework formalizing the thermodynamic properties of reactive species formed during the solvolysis, as the solvent itself changes its polymerization properties upon introduction of other oxide components, which are highly soluble contrary to what observed for salts in aqueous solutions. The most general thermodynamic approaches postulate mineral-like molecular structures to interpolate existing data.

In molten silicates the electric charge is primarily transported by cations, whose contribution increases with concentration of network modifiers, hence basicity. The major element, oxygen in its three forms and particularly O^{2-} and O-based anionic complexes do not contribute substantially to the charge transport (Dickson and Dismukes, 1962; Dancy and Derge, 1966; Cook and Cooper, 1990, 2000; Cooper et al., 1996a,b; Magnien et al., 2006, 2008; Cochain et al., 2012, 2013; Le Losq et al. 2020). This is a striking difference when comparing silicate melts

to previously described electrolytes, particularly with the aqueous electrolytes, in which the concentration of hydroxide ions or water is always large enough to sustain high current densities (Allanore, 2013). From a practical standpoint the anode reaction producing oxygen (the inverse of Reaction 1.6) is strongly impacted by the low transport of free oxide ions, that is free oxygen, which is at very low concentration. Besides, the anode design and technical performance would greatly benefit of the precise knowledge of oxygen physical chemistry in silicate melts, which for the moment is still too limited to narrow compositional ranges that have been investigated spectroscopically (Allanore, 2015).

Nevertheless, because of their nature, silicate melts can dissolve important amounts of metals. Besides, they exhibit a large range of thermal stability, with high temperature conditions that favor fast kinetics of redox exchanges. Upper temperature limits for electrochemical applications are given by the formation of gaseous silicon monoxide or by alkali oxide thermal decomposition in alkaline systems or by high vapor pressure for Mn-bearing systems (Allanore, 2015). In terms of transport properties, silicate melts are a solvent with high viscosity, a fact that is however compensated by the high diffusivity of the metal cation (Allanore, 2013), i.e., the cathode reactant.

Many measurements have however been carried out on melts of geological interest, also fostered by the interest in silicate electrolysis to produce on site metals and particularly molecular oxygen for terraformation of extraterrestrial planets (e.g., Haskin et al., 1992). Electrochemical series were then established in binary SiO_2-MO systems (e.g., Schreiber, 1987) but also in ternary joins such as the diopside one (Semkow and Haskin 1985; Colson et al., 1990) for redox exchanges of the type:

$$4M^{m+}_{'(melt)} + 2nO^{2-} \Leftrightarrow 4M^{(m-n)+}_{(melt)} + nO_{2(gas)} \quad (1.39)$$

in which half-reactions of the type

$$M^{m+}_{'(melt)} + ne^{-} \Leftrightarrow M^{(m-n)+}_{(melt)} \quad (1.40)$$

combine with Half-reaction 1.7. Nevertheless, such series do not consider the effect of the solvent, the melt and its structure, in determining the speciation state (e.g., anionic or cationic) following the definition at Reaction 1.27. The effect of the solvent also includes the amphoteric behaviour of some dissolved oxides such as Fe_2O_3 or Eu_2O_3, which can behave either as acids, yielding FeO_2^- (i.e., FeO_4^{5-} tetrahedral units) and EuO_2^- (i.e., EuO_4^{5-}) or bases, yielding Fe^{3+} and Eu^{3+} cations (Fraser, 1975; Ottonello et al., 2001; Moretti, 2005; Le Losq et al., 2020). The multiple speciation behaviours determined by pO^{2-} can be summarized by the following reaction mechanism (e.g., Moretti, 2005; Pinet et al., 2006):

$$MO^{(2x-m)-}_{x,melt} \Leftrightarrow MO^{(2y-m+n)-}_{y,melt} + \left(x - y - \frac{n}{2}\right)O^{2-} + \frac{n}{4}O_2 \quad (1.41)$$

Predominance and stability diagrams (e.g., E-pH, E-pO^{2-}, E-logfO_2, or logfO_2 vs. the log-fugacity of pH or other gaseous species in the system such as SO_2, CO_2) depend on the availability of good thermodynamic data and especially a well-established testament of acid-base properties of the investigated system and its solvent(s). For silicate melts and glasses, such a testament is represented by the oxobasicity scale from the Lux definition (Reaction 1.27). Electrochemical experiments should then be envisioned to complete and validate the database in order to ensure predictions about forming species and measure their activities.

1.2. OXYGEN FUGACITY: THE CENTRALITY OF AN ELUSIVE PARAMETER

Voltage E and oxygen fugacity (fO_2) are both measures of oxidation state. The relation between fO_2 and E for a given electrolytic medium can be established by the anode reaction where oxygen is produced. In the case of aqueous solutions, conversion is provided by half-reaction 1.15 and Equation 1.18. We can then replace E-pH diagrams with analogous logfO_2-pH diagrams. In this treatment, the actual speciation state of solutions is still the key to investigate the system, but half-reactions are not considered, and the equilibrium values of overall reactions are used, same as for activity plots. As for E-pH plots, boundaries will shift by varying the total amount of soluble elements in the electrolytic solution, hence the activity of dissolved ionic species or the corresponding gas fugacity (e.g. when carbonates or sulfides and sulfates are present).

Figure 1.4 shows that in logfO_2-pH diagrams phase, boundaries that in E-pH diagrams were dependent on pH only (and not on the concentration of dissolved ions) are horizontal. Moreover, a quick comparison between figures 2 (Eh-pH diagram) and 4 (logfO_2-pH diagram) also shows that on the logfO_2 vs. pH representation the pyrite–magnetite boundary, which appears only for pH > 7, maintains the positive slope. At the T conditions of Figure 1.4 this boundary is represented by the overall reaction:

$$3FeS_{2(S)} + 6H_2O_{(aq)} \Leftrightarrow Fe_3O_{4(s)} + 6HS^-_{(aq)} + 6H^+_{(aq)} + O_2 \quad (1.42)$$

Besides, at 145°C (water saturated conditions) the pyrite–pyrrhotine boundary is defined at pH > 7 and is positive because:

$$FeS_2 + 2H_2O \Leftrightarrow FeS + 2HS^- + 2H^+ + O_2 \quad (1.43)$$

whereas for pH < 7 the boundary is horizontal, given by the proton-free reaction:

$$FeS_2 + H_2O_{(aq)} \Leftrightarrow FeS + H_2S_{(aq)} + \tfrac{1}{2}O_2 \qquad (1.44)$$

As we have already seen, when considering high-temperature non-aqueous (oxide) systems in the inner Earth geospheres, there is no acid–base framework and anchoring fO_2 or E to pH makes no sense in absence of the solvent liquid water.

To measure the chemical potential of redox exchanges in higher temperature geological systems, geoscientists turned their attention to molecular oxygen transfer among molecular components such as oxides or mineral-like macromolecular entities.

The practice between geoscientists becomes to assess criteria for fO_2 (or aO_2) estimations disconnected from the formal description of the acid–base character of magmas. In particular, techniques were established involving mineral phases coexisting in igneous rock to establish thermodynamic or empiric laws and trends from quenched glasses via indirect measurements, most often of spectroscopic nature (e.g., Neuville et al., 2020). This change of perspective reflects the obvious consideration that geoscientists deal with samples (solidified rocks) made accessible at Earth's surface and which represent the final snapshots at the end of a long thermal and chemical evolution, whose *a posteriori* reconstruction is the objective of the geochemical (*lato sensu*) investigation.

We may then say that for practical reasons geoscientists remained anchored to the original Lavoisier-like definition of oxidation occurring in combustion processes, related to the exchange of oxygen molecules. The fact that most of the chemical analyses were from techniques in which oxygen was not directly determined but allowed to give oxides has also further favored these approaches.

In this framework, a mutual exchange of knowledge has always characterized the field of geochemistry and petrology on one side and that of metal extraction in metallurgy in the other. Relations of the type

$$M^{\nu+}{}_{2/\nu}O_{(s/l)} \Leftrightarrow 2/\nu M_{(s/l)} + 1/2O_{2(g)} \qquad (1.45)$$

with v the charge (positive) of the cation of the metal M in the corresponding oxide. Reaction 1.45 is the main target of extractive metallurgy (see also Reaction 1.34), but also sketches the ensemble of processes that occurred since early Earth's evolution to segregate the metallic core.

Ellingham diagrams (Ellingham 1944; Figure 1.5) are used in metallurgy to evaluate the ease of reduction of metal oxides, as well as chlorides, sulfides, and sulfates. The diagram shows the variation of the standard Gibbs free energy of formation, ΔG^0, with temperature for selected oxides and is used to predict the equilibrium temperature for reactions of the type of Reaction 1.45 and particularly the oxygen fugacity under which ore will be reduced to its metal. The standard Gibbs energy change of formation of a compound (the Gibbs energy change when one mole of a compound is formed from elements at P = 1 bar) is given by:

$$\Delta G_f^0 = \Delta H_f^0 - T\Delta S_f = \left[\Delta H_{298}^0 + \int_{298}^{T} CpdT\right] - T\left[\Delta S_{298} + \int_{298}^{T} \frac{\Delta Cp}{T} dT\right] = A + B \times T(K) \qquad (1.46)$$

with R the universal gas constant and A and B constants.

To compare the relative stabilities of the various oxides, the Ellingham diagram is prepared for oxidation reactions involving one mole of oxygen. For the oxidation of a metal, ΔG^0 represents the chemical affinity of the metal for oxygen. When the magnitude of ΔG^0 is negative, the oxide phase is stable over the metal and oxygen gas. Furthermore, the more negative the value, the more stable the oxide is. The Ellingham diagram also indicates which element will reduce which metal oxide. The similarity between the electromotive force series (E^0) and the Ellingham diagram, which rates the tendency of metals to oxidize, should be easily recognized.

When both Me and $Me^{\nu+}{}_{2/\nu}O$ in Reaction 1.45 are in their standard states, the equilibrium constant, K_{45}, corresponding to this reaction can be expressed as:

$$K_{45} = aM^{2/\nu}{}_{(s/l)}/aM^{\nu+}{}_{2/\nu}O_{(s)} \cdot 1/aO_2 = (f^0O_2/fO_2)^{1/2} \qquad (1.47)$$

where $fO_2{}^0$ is the pure gas component gas fugacity at standard state (in this case 1 bar and T of interest). If, at any temperature, the acting oxygen fugacity is greater than the calculated value from Equation 1.47, spontaneous oxidation of metal M occurs, while oxide $Me^{\nu+}{}_{2/\nu}O_{(s)}$ decomposes to metal Me and gaseous oxygen at the oxygen partial pressure less than the equilibrium value. In other words, an element is unstable, and its oxide is stable at higher oxygen potentials than its $\Delta G_f{}^0$–T line on the Ellingham diagram. Therefore, the larger negative value for $\Delta G_f{}^0$ an oxide has, the more stable it is. In the Ellingham diagram of Figure 1.4, it can be seen, for example, that the reduction of Cr_2O_3 by carbon is possible (from the thermodynamic standpoint) at temperature above 1250°C and at each reported temperature by aluminum. It is worth noting that the Ellingham line for the formation of carbon monoxide (CO) has a negative slope, while those of all other oxides have positive slopes. As a result, at sufficiently high

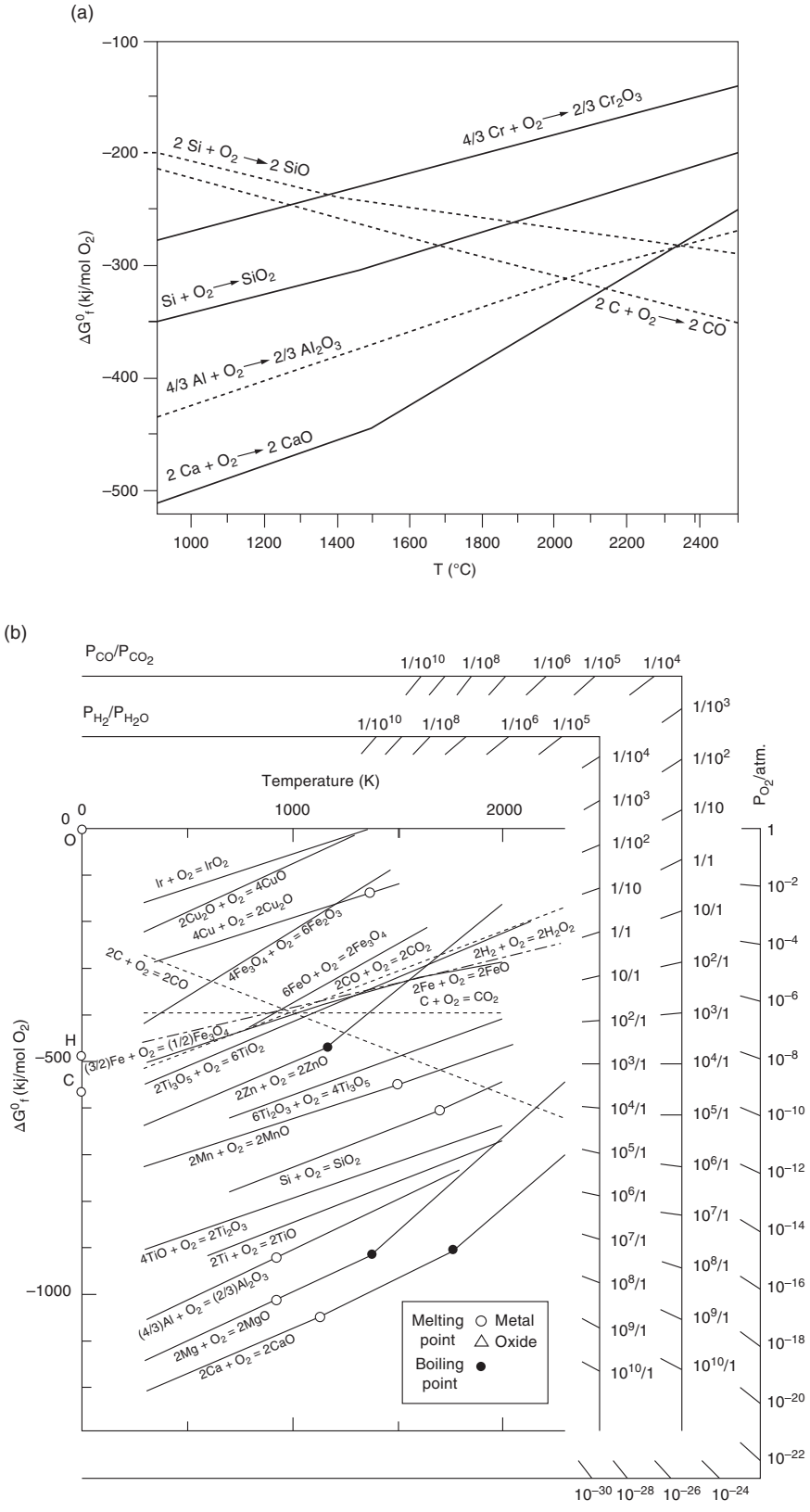

Figure 1.5 **(a)** Ellingham diagram for the main components of the melt/slag (solid lines) and possible reducing agents (dotted lines). The slopes of the lines representing ΔG_f^0–T relations change at the temperature in which the phase transformations of reactants or products occur. Modified from Zhang et al. (2014). **(b)** Full Ellingham diagram for some relevant oxides including CO_2 equilibria and normographic scales for oxygen fugacity and related quantities via CO/CO_2 and H_2/H_2O ratios at P_{tot} = 1 bar. The scale of P_{H_2}/P_{H_2O} ratio is used in the same manner as that of P_{CO}/P_{CO_2} ratio, except that the point H on the ordinate at T= 0 K is used instead of point C. Modified from Hasegawa (2014). All reactions' components are considered in their pure stable phase t 1 bar and T of interest.

temperatures, carbon will reduce even the most stable oxides.

Reaction 1.45 illustrates in fact how pairs of metals and their oxides, both having unitary activity, can be used as redox buffers, such that fO_2 values can be easily fixed at any temperature. Even in the presence of a third phase, such as silicate melts or any other liquid, gas–solid assemblages allow a straightforward application of Equation 1.47 to impose fO_2, unless solid phases are not refractory, and dissolve other components exchanges with the coexisting liquid. Reaction 1.1, involving metal iron and wustite, is a typical example (so-called IW buffer) of one of these gas–solid equilibria fixing fO_2.

In order to illustrate the effect of the fluid phase, refined versions of the Ellingham diagrams included normographic scales, which are designed so that the equilibrium oxygen partial pressure or the corresponding P_{H_2}/P_{H_2O} or P_{CO}/P_{CO_2} ratios between metal and its oxide can be read off directly at a given temperature by drawing the line connecting point O for P_{O_2}, C for P_{CO}/P_{CO_2}, or H for P_{H_2}/P_{H_2O} in Figure 1.5 and the condition of interest (Reaction 1.45 at T of interest) and then extending it to the corresponding normographic scale.

It is now quite obvious to see how both metallurgists and petrologists could then develop techniques to constrain fO_2 to investigate melting and sub-solidus conditions of oxides and silicates. After the seminal studies of Bowen and Schairer (1932, 1935) on $FeO–SiO_2$ and $MgO–FeO–SiO_2$ systems and in which the authors used iron crucibles in an inert (O_2-free) atmosphere to equilibrate the phases with metallic iron at very low but also unknown P_{O2}, early fO_2 control techniques were applied by Darken and Gurry (1945, 1946), who detailed the Fe–O system based on the use of CO and CO_2, or CO_2 and H_2, conveyed in a gas-mixer supplying a continuous mixture in definite constant volume proportions.

Later Eugster, in his early experiments to determine the phase relations of annite had to prevent its oxidation and formation of magnetite (Eugster 1957, 1959; Eugster and Wones 1962). He then developed the double capsule technique, with a Pt capsule containing the starting material, surrounded by a larger gold capsule. A metal–oxide or oxide–oxide pair plus H_2O was then placed between the two metal containers. In these experiments, reaction involving OH-bearing minerals and H_2O provides a fixed and known hydrogen fugacity (Eugster 1977), so through the dissociation Reaction 1.14 measurement of fH_2 allows calculating both fO_2 given the fH_2O at the experimental pressure ($aH_2O = 1$)of the internal capsule.

Since Eugster, many metal–oxide and oxide–oxide assemblages have been used in experimental petrology that have been called "redox buffers." These buffers have contributed to our understanding of the role of fO_2 on melt phase equilibria and mineral composition on Earth, also under volatile saturated conditions due to the possibility of evaluating fluid phase speciation at the experimental P and T conditions (e.g., Pichavant et al., 2007; Frost and McCammon, 2008. Mallmann and O'Neill, 2009; Feig et al., 2010). The results of experimental petrology made it possible to systematically collect glasses (quenched melts) to measure ratios of metals in their different oxidation states, particularly Fe^{II}/Fe^{III}, and relate such ratios to experimental P, T, and fO_2, glass composition, or other spectroscopic observations about glass/melt structure and the local coordination of targeted metals (Neuville, 2020 and references therein).

Obviously on Earth iron is the most abundant multivalent element and because of its speciation behaviour it gives rise to many reactions involving minerals and liquid (i.e., natural melts, particularly silicate ones). Reactions such as Reaction 1.1 are then useful for providing a scale with geological significance for fO_2 conditions that are recorded in rock and minerals formed in past and present Earth environments, from the core (in which Fe^0 dominates) up to shallow crust and through all igneous environments where it exists, and Fe^{II} and Fe^{III}. To provide systematics for the aO_2 conditions the following gas–solid reactions, other than Reaction 1.1, were then assessed (Figure 1.6):

$$4Fe_3O_4 + O_2 \Leftrightarrow 6Fe_2O_3 \,(\text{magnetite} – \text{hematite; MH}) \tag{1.48}$$

$$3Fe_2SiO_4 + O_2 \Leftrightarrow 2Fe_3O_4 + 3SiO_2 \,(\text{fayalite} – \text{magnetite} – \text{quartz; FMQ}) \tag{1.49}$$

$$3FeO + O_2 \Leftrightarrow Fe_3O_4 \,(\text{wustite} – \text{magnetite; WM}) \tag{1.50}$$

$$SiO_2 + 2Fe + O_2 \Leftrightarrow Fe_2SiO_4 \,(\text{iron} – \text{quartz} – \text{fayalite; IQF}) \tag{1.51}$$

All these equilibria have the interesting feature of displaying unitary activities for oxide component appearing as pure phases, such that their equilibrium constants simply describe the variations of O_2 activity (aO_2) with temperature:

$$\log fO_2 = A/T + B \tag{1.52}$$

or, by defining fugacity, with temperature and pressure:

$$\log fO_2 = A/T + B + C(P-1)/T \tag{1.53}$$

with A, B, and C constants. The pressure term, C, allows computing directly fO_2 rather than aO_2 at the pressure of interest. Mineral assemblages making up Reactions 1.1 and 1.44 to 1.47 are not necessarily occurring in deep Earth and igneous environments, whereas the actual multi-component space of phases fix the aO_2 via multiple equilibria in which solid solutions and/or the presence of

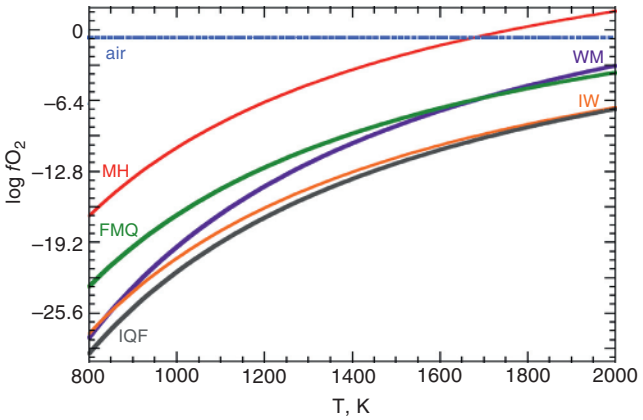

Figure 1.6 Common solid oxygen buffers used in petrology and geochemistry. The lines represent the fugacity-temperature conditions where the phases coexist stably. FMQ: fayalite, magnetite, quartz; IW: iron–wüstite; WM: wüstite–magnetite; HM magnetite–hematite. Oxygen fugacity values were computed for a total pressure of 1 bar. Also reported is the value of logfO_2 in air (PO_2 ~0.21 bar).

relatively mobile liquid (silicate melts) and/or supercritical fluids play a fundamental role.

However, when one of these mineral "buffers" is selected as a reference, the acting logfO_2 can be given as a relative value, without temperature:

$$\Delta buffer = \log fO_2 - \log fO_{2,\text{buffer}} \qquad (1.54)$$

A relative fO_2 scale embodying temperature effects bears just a practical implication (tracking fO_2 variations with respect to a reference) but not a real meaning about logfO_2 evolution in igneous systems and related environments (e.g., Moretti and Steffansson, 2020). In particular, a common misconception was that in a system a given value of $\Delta buffer$ (e.g., ΔQFM = 0.5) could represent some kind of "magic number" characteristic of the whole "rock system" throughout its thermal and chemical evolution. In natural environments oxygen activity (hence fugacity) in fact varies to accommodate the compositional variations and the speciation state of the mineral/melt/fluid phases, and also when highly mobile volatile components are involved, such that fO_2 can thus be fixed by factors that are external to the system object of the thermodynamic description.

Similarly, the rock system evolution cannot be approximated by a unique Fe^{II}/Fe^{III} ratio, that the system had when completely molten. Indeed, two rocks that have ideally crystallized along the QFM buffer may have different proportions of fayalite ad magnetite because of the crystallization style but different Fe^{II}/Fe^{III} bulk ratios (Frost, 1991). However, in some systems, it is possible that the melt fixed the redox potential of the system via iron oxidation state, with the Fe^{II}/Fe^{III} ratio approaching unity (e.g. Moretti et al., 2013).

It is also important to recall that fO_2 is just a thermodynamic parameter used to conveniently report the oxidation state of a system, particularly when O_2 is not an existing gaseous species that could be detected if the system were accessible to measurements. This is clearly proved by the very low values reported in ordinates in Figure 1.6. Therefore, fO_2 turns out to be by-product of thermodynamic calculations applied to the analyses from natural samples, in which the true redox observables are the oxidation states of iron and other elements in minerals and liquids. The common practice is then to measure the concentration ratio of redox couples of multiple valence elements in melts (Fe^{II}/Fe^{III}, but also S^{-II}/S^{VI}, V^{III}/V^{V}, etc.) or in gases (e.g., H_2/H_2O, CO/CO_2, H_2S/SO_2) and relate them to fO_2 via thermodynamic calculations using appropriate standard state thermochemical data. As fO_2 is provided, its value is then anchored via Equation 1.54 to a given gas-solid buffer of the Reaction type 1.1 or 1.48 to 1.51. This is quite easy for gases, in which governing equilibria are directly solved if the gas analysis is provided (e.g., Giggenbach, 1980, 1987; Aiuppa et al., 2011 and references therein) and also for solid–solid equilibria, such as in case of coexisting iron–titanium oxide solid solutions titanomagnetite (Fe_3O_4-Fe_2TiO_4) and hemo-ilmenite (Fe_2O_3–$FeTiO_3$) (Buddington and Lindsley, 1964) or for peridotite assemblages in the mantle (e.g., Mattioli and Wood, 1988; Gudmundsson and Wood, 1995), in which the good thermodynamic characterization of solid solutions allows quite accurately treating component activities, based on mineral analyses.

On the contrary, it is much less straightforward for fO_2 estimates by oxidation states of Fe and/or S measured in glasses, as the oxybarometers derived by the study of synthetic quenched melts still suffer from too many empiric approaches. Because of their polymerized nature, silicate melts do not allow a precise distinction between solute and solvent like in aqueous solutions, where complexes and solvation shells can be easily defined in which covalence forces exhaust (see also Moretti et al., 2014). In fact, melt composition largely affects the ligand constitution and then the speciation state of redox-sensitive elements. In the case of the Fe^{II}/Fe^{III} ratio, the most common redox indicator for melts/glasses, the choice of components in reaction:

$$FeO_{(m)} + 1/4O_2 \Leftrightarrow FeO_{1.5(m)} \qquad (1.55)$$

over a large compositional range (e.g., from mafic to silicic) does not offer the possibility to find accurate and internally consistent expressions for the activity coefficients of *oxide components* γFeO and $\gamma FeO_{1.5}$ (with $FeO_{1.5}$ conveniently replacing Fe_2O_3) that solve the reaction equilibrium constant:

$$\log fO_2 = 4\log\frac{X\mathrm{Fe^{III}}}{X\mathrm{Fe^{II}}} + 4\log\frac{\gamma\mathrm{FeO_{1.5}}}{\gamma\mathrm{FeO}} + \frac{\Delta G^0_{1,T} + \int_1^P \Delta V_{FeO_{1.5}-FeO}\,dP}{2.303RT} \quad (1.56)$$

in which the term within integral is the difference of partial molar volumes of iron components. Expansion of excess contribution to its Gibbs free energy of mixing is used to define γFeO and $\gamma FeO_{1.5}$ in melt mixtures. However, when these are adopted to solve Equation 1.56 for measured Fe^{II}/Fe^{III} values, they show success only over limited compositional datasets (Moretti, 2020 and references therein). Armstrong et al. (2019) calibrated volumes and interaction parameters of activity coefficients entering equation (1.56) for an andesitic melt (easily quenchable as a glass) with fO_2 buffered by the Ru-Ru_2O assemblage in the T-range 1673K to 2473K and for pressures up 23 GPa. Data fitting showed that volume term in Equation 1.56 turns from negative to positive for P > 10 GPa, which yielding iron oxidation with increasing pressure. The calibrated Equation 1.56 was then used by the authors to demonstrate how the mantle oxidized after the Earth's core started to form by a deep magma ocean with initial $Fe^{III}/Fe_{tot} = 0.04$ from which FeO disproportionated to Fe_2O_3 plus metallic iron at high temperature. The separation of Fe^0 to the core raised the oxidation state of the upper mantle and of exsolved gases that were forming the atmosphere (Armstrong et al., 2019).

The search for one general formulation for all melt compositions of interest in petrology and geochemistry led to empirical expressions, in which adjustable parameters are introduced without the formal rigor requested by Equation 1.56 (e.g. Kress and Carmichael, 1991). These formulations furnish quite accurate fO_2 values from measured Fe^{II}/Fe^{III} ratios within the compositional domain in which they have been calibrated. Besides, they often violate reaction stoichiometry and do not ensure internal consistency: if used to calculate activities they fail the application of the Gibbs-Duhem principle relating all component activities within the same phase (e.g., Lewis and Randall, 1961). Such expressions then treat fO_2 as a Maxwell's demon, doing what we need it to do to fit the calibration data and with the consequence that outside the calibration domain, all the unpredictable non-idealities are discharged on the fO_2 terms, resulting in biased calculations of fluid speciation, or other phase equilibria constraints.

As extensively treated in Moretti (2020), unpredictable non-idealities reflect counterintuitive behaviors that cannot be accounted for by activity coefficients used in the equilibrium constant of Reaction 1.55. It is well known that depending on melt composition alkali addition (i.e. decreasing pO^{2-}) can either oxidize or reduce iron in the melt. This occurs because of the change of speciation due to the amphoteric behavior of Fe^{III}, which depending on composition and then pO^{2-} can behave as either network former or modifier (see the conceptualization provided by Ottonello et al., 2001; Moretti, 2005, 2020; Le Losq et al., 2020; see also Reaction 1.41). Models that define the melt (oxo)acidity (Reaction 1.27) hence pO^{2-} (e.g; polymeric models based on the Toop and Samis mixing of bridging, non-bridging and free oxygens; see Moretti, 2020, and references therein) allows solving speciation and set activity-composition relations of ionic and molecular species, just as for aqueous solutions and molten salts.

The problem of unsolved compositional behaviors due to speciation, that are not accounted for by typical oxide-based approaches to mixtures, is exacerbated when dealing with the mutual exchanges involving iron and another redox-sensitive elements, such as sulfur. Sulfur-bearing melt species play a special role since the oxidation of sulfide to sulfate involves eight electrons: for any increment of the Fe^{III}/Fe^{II} redox ratio, there is an eight-fold increment for sulfur species (S^{-II}/S^{VI}; e.g., Moretti and Ottonello, 2003; Nash et al., 2019; Cicconi et al., 2020b; Moretti and Stefansson, 2020). Sulfur in magmas partitions between different phases (gas, solids such as pyrrhotite and anhydrite, and liquid as well, such as immiscible Fe–O–S liquids; Baker and Moretti, 2011 and references therein). The large electron transfer makes S^{-II}/S^{VI} a highly sensitive indicator to fO_2 changes in a narrow range (typically around QFM and NNO buffers in magmatic melts; Moretti, 2020 and references therein), whereas its effectiveness as a buffer of the redox potential is limited by the abundance of sulfur in magma, significantly lower than iron.

The modelling of joint Fe and S redox exchanges is still a major challenge which sees contrasting approaches (see Moretti, 2020). Formulations exist with various degrees of empiricism, but even those displaying better performances in exploring the $fO_2 - fS_2$ space of natural silicate melts (Moretti and Baker, 2008) should be carefully tested in reproducing phase diagrams involving multiple phases, including coexisting Fe–O–S melt, $FeS_{(s)}$, and $Fe_3O_{4(s)}$. Introduction of sulfur equilibria in petrogenetic grids would be a major step forward for modelling in igneous petrology. Besides, it would provide the liaison with processes occurring in late- to post-magmatic stages, prior to further cooling down to real hydrothermal conditions dominated by condensed water (see Figure 1.4). For late- to post-magmatic stages, such as in the case of porphyry-copper ore formation, $\log fO_2$-$\log fS_2$ diagrams. Figure 7 reliably summarizes phase relations in the Fe–S–O system, in a way similar to Figure 1.2 and 1.4. It is worth noting that the diagram in Figure 1.7 can also be seen as resulting from reactivity of a sub-solidus mixed iron

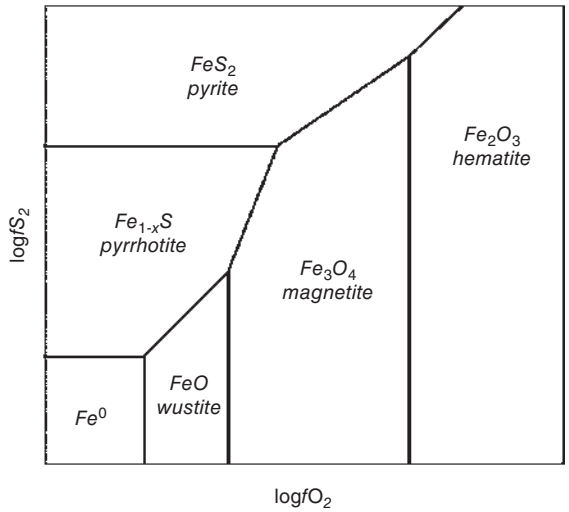

Figure 1.7 Two-redox potential fO_2-fS_2 diagram. The conformation of stability fields in the Fe–O–S space is essentially the same also for large fO_2 and fS_2 variations with temperature (redrawn from Nadoll et al., 2011).

molten oxide–sulfide, in which the two main ligands are O^{2-} and S^{2-} (half-reactions 1.6, 1.11, and 1.12).

A natural assemblage of pyrite + magnetite + pyrrhotite corresponds then to the triple point marked by a star in Figure 1.7, which at a given T is invariant for fO_2 and fS_2 values given by the simultaneous occurrence of Reaction 1.10 and:

$$Fe_3O_{4(s)} + 3FeS_{2(s)} \Leftrightarrow 6FeS_{(s)} + O_2 \qquad (1.57)$$

that allow identifying the stable phase as a function of temperature and fugacities (or activities) of reference gas species. It is worth noting that in absence of water (no H in the system represented in Figure 1.7) the boundary between FeS_2 and FeS is a function of fS_2 only (see Reaction 1.10) but not of fO_2, as instead reported in Figure 1.4.

1.3. CONCLUDING REMARKS AND PERSPECTIVES

In this short compendium we show the redox features in aqueous-hydrothermal and igneous Earth. This allows the summarizing of the main redox features of a system, to show what we know of its equilibrium properties, but also what we do not know, especially for melts and magmas. We make a parallel between redox in magmas and redox in aqueous-hydrothermal solutions and show that what really changes is the way redox variables are reported. It is better described in aqueous solutions, via E-pH relations, because of the sound knowledge of acid–base properties, which allows good prediction of system reactivity with compositional changes and fosters applications in water-based geochemistry and industrial practice (e.g. corrosion and hydrometallurgy).

Just as the measurement of pH is the key to studies of acid–base reactions, those of reactions involving the O^{2-} ion in silicate melts naturally go through the measurement of pO^{2-}, a magnitude similar to pH and playing an identical role. Same as a pH indicator electrode, a pO^{2-} indicator electrode is the essential instrument to study acid–base properties of silicate melts. Technical challenges exist about this electrode as an instrument of analytical control operating directly in melts at high temperature and also as working assembly for anode reaction (inverse of Reaction 1.6). Besides, the low flux of oxide ion compared to cations is limited in melts and the lack of physical and chemical information about the molecular entities involved in the transport processes at each electrode and in the bulk of the electrolyte presents a conceptual difficulty for engineering the electrodes (Allanore et al., 2015).

Contrary to waters, in which E-pH pairs can be measured in the field by probe electrodes and then directly compared to theoretical assessments, magma-related samples do not offer the possibility to probe the conditions (temperature, pressure, gas composition, and also phase proportion) under which they equilibrated before becoming accessible to our observations. These conditions cannot be restored and must be calculated under strong assumptions, for example that glasses have preserved the same oxidation state of the melt from which they quenched. The impossibility to restore and measure the original system has surely contributed to overlooking the role played by acid–base properties and resulted in oxide-based redox descriptions of melts and magmas centred around the thermodynamic concept of fO_2, whose sole adoption was boosted by experimental petrology and the thermodynamic approach based on Ellingham's diagrams in extractive metallurgy. The acid–base concept was progressively relegated to qualitative assessments (e.g., silicic for acidic and mafic for basic).

With the exception of volcanic gases, where fO_2 (or related quantities such as fH_2) can be directly measured with solid-state O_2 electrodes (Aiuppa et al., 2011 and references therein), the common practice, recently boosted by advancements in microbeam spectroscopic techniques (e.g., XANES) is to measure masses of elements in their different oxidation state and then relate such ratios to fO_2 via approaches either based on thermodynamics or having a thermodynamic flavour to solve for the role of composition. Nevertheless, such approaches are valid only in limited compositional ranges and discharges on calculated fO_2 the non-ideal behaviours that are determined by speciation, hence by pO^{2-}, and which

cannot be reproduced by interaction parameters of oxide components (see Moretti, 2020).

These unpredictable non-ideal behaviours are reflected by the shape of the excess Gibbs free energy of mixing, which is correctly reproduced only by ionic-polymeric approaches to silicate melts mixing properties (e.g., Mao et al., 2006; Hillert et al., 1985; Ottonello and Moretti, 2004), which formalize the role of composition in establishing the relationships between polymerization and redox state in the melt. These approaches could be in perspective used to generate pO^{2-} based phase diagrams, particularly $\log fO_2$-pO^{2-} diagrams analogous to $\log fO_2$-pH ones reported in Figure 1.4 for aqueous-hydrothermal solutions.

The joint description of acid–base properties and redox exchanges via predominance and stability diagrams would reduce ambiguities about the role of redox state and the "*who controls what*" dilemma: is fO_2 a rather elusive parameter, or is it the bulk composition in the system that fixes the observed redox state? Besides, they would help in providing a more complete and formal redox description of geodynamic settings, in particular of how the redox state of magmas is a reflection of the source signature or the result of subsequent modifications due to magma evolution via partial melting, fractional crystallization, assimilation, or degassing (Carmichael, 1991; Burgisser and Scaillet, 2007; Gaillard et al., 2015; Moretti and Stefansson, 2020 and references therein) whose understanding would be beneficial at the scale of a single volcanic system to improve the forecasting of eruptions at both open-conduit (generally basaltic) and closed-conduit (generally andesitic) volcanoes via gas monitoring. Besides, this would better constrain the role of redox state on Earth's evolution since its formation and accretion.

ACKNOWLEDGMENTS

We thank Alexander Pisch (SIMAP, CNRS, France) and Maria Rita Cicconi (FAU, Germany) for their valuable reviews. The precious support of AGU Books editorial staff is greatly acknowledged. This study contributes to the IdEx Université de Paris ANR-18-IDEX-0001.

REFERENCES

Aiuppa, A., Shinohara, H., Tamburello, G., Giudice, G., Liuzzo, M., & Moretti, R. (2011). Hydrogen in the gas plume of an open-vent volcano, Mount Etna, Italy. *Journal of Geophysical Research: Solid Earth*, *116*(B10). https://doi.org/10.1029/2011JB008461

Allanore A. (2013). Electrochemical engineering of anodic oxygen evolution in molten oxides. *Electrochimica Acta*, *110* (2013), 587–592.

Allanore A. (2015). Features and challenges of molten oxide electrolytes for metal extraction. *Journal of the Electrochemical Society*, *162*, E13–E22. https://doi.org/10.1149/2.0451501jes

Appelo C. A. J., & Postma, D. (1996). *Geochemistry, groundwater and pollution*. Rotterdam: Balkema. 536 pp.

Armstrong, K., Frost, D. J., McCammon, C. A., Rubie, D. C., & Ballaran, T. B. (2019). Deep magma ocean formation set the oxidation state of Earth's mantle. *Science*, *365* (6456), 903–906. doi: 10.1126/science.aax8376

Baker, D. R., & Moretti, R. (2011). Modeling the solubility of sulfur in magmas: a 50-year old geochemical challenge. *Reviews in Mineralogy and Geochemistry*, *73*(1), 167–213. https://doi.org/10.2138/rmg.2011.73.7

Barton, P. B., Jr. (1970). Sulfide petrology: Mineralogical Society of America Special Paper 3, 187–198.

Biernat R. J., & Robins, R. G. (1969). High temperature potential/pH diagrams for the sulfur-water system. *Electrochimica Acta 14*, 809–820. https://doi.org/10.1016/0013-4686(69)87003-9

Bowen, N. L., & Schairer, J. F. (1932). The system, FeO-SiO 2. *American Journal of Science*, *141*, 177–213. https://doi.org/10.2475/ajs.s5-24.141.177

Bowen, N. L., & Schairer, J. F. (1935). The system MgO-FeO-SiO 2. *American Journal of Science*, *170*, 151–217. doi: 10.2475/ajs.s5-29.170.151

Buddington, A. F., & Lindsley, D. H. (1964). Iron-titanium oxide minerals and synthetic equivalents. *Journal of Petrology*, *5*, 310–357. https://doi.org/10.1093/petrology/5.2.310

Burgisser, A., & Scaillet, B. (2007). Redox evolution of a degassing magma rising to the surface. *Nature*, *445*(7124), 194–197. https://doi.org/10.1038/nature05509

Carmichael, I. S. (1991). The redox states of basic and silicic magmas: a reflection of their source regions? *Contributions to Mineralogy and Petrology*, *106*(2), 129–141. https://doi.org/10.1007/BF00306429

Casey H. W. (2017). Oxidation-Reduction Reactions and Eh-pH (Pourbaix) Diagrams. In: W.M. White (ed.), *Encyclopedia of Geochemistry*, doi:10.1007/978-3-319-39193-9_21-1

Cicconi, M. R., Moretti, R., & Neuville, D. R. (2020a). Earth's Electrodes. *Elements*, *16*, 3, 157–160. doi: 10.2138/gselements.16.3.157

Cicconi, M. R., Le Losq, C., Moretti, R., & Neuville, D. R. (2020b). Magmas are the largest repositories and carriers of Earth's redox processes. *Elements*, *16*, 3, 173–178. doi: 10.2138/gselements.16.3.173

Colson, R. O., Haskin, L. A., & Crane, D. (1990). Electrochemistry of cations in diopsidic melt: Determining diffusion rates and redox potentials from voltammetric curves. *Geochimica et Cosmochimica Acta*, *54*, 3353–3367. https://doi.org/10.1016/0016-7037(90)90290-2

Cochain B., Neuville D. R., Henderson G. S., McCammon C., Pinet O., & Richet, P. (2012). Iron content, redox state and structure of sodium borosilicate glasses: A Raman, Mössbauer and boron K-edge XANES spectroscopy study. *Journal of the American Ceramics Society*, *94*, 1–12. https://doi.org/10.1111/j.1551-2916.2011.05020.x

Cochain, B., Neuville, D. R., de Ligny, D., Malki, M., Testemale, D., Pinet O., & Richet P. (2013). Dynamics of iron-bearing borosilicate melts: Effects of melt structure and composition on viscosity, electrical conductivity and kinetics of

redox reactions. *Journal of Non-Crystalline Solids*, *373–374*, 18–27. https://doi.org/10.1016/j.jnoncrysol.2013.04.006

Cook, G. B., & Cooper, R. F. (2000). Iron concentration and the physical processes of dynamic oxidation in alkaline earth aluminosilicate glass. *American Mineralogist*, *85*, 397–406. https://doi.org/10.2138/am-2000-0401

Cook, G. B., Cooper, R. F., & Wu, T. (1990). Chemical diffusion and crystalline nucleation during oxidation of ferrous ironbearing magnesium aluminosilicate glass. *Journal of Non-Crystalline Solids*, *120*, 207–222. https://doi.org/10.1016/0022-3093(90)90205-Z

Cooper, R. F., Fanselow, J. B., & Poker, D. B. (1996a). The mechanism of oxidation of a basaltic glass: chemical diffusion of network-modifying cations. *Geochimica et Cosmochimica Acta*, *60*(17), 3253–3265. https://doi.org/10.1016/0016-7037(96)00160-3

Cooper, R. F., Fanselow, J. B., Weber, J. K. R., Merkley, D. R., & Poker, D. B. (1996b). Dynamics of oxidation of a Fe2+-bearing aluminosilicate (basaltic) melt. *Science*, *274*, 1173–1176. doi: 10.1126/science.274.5290.1173

Darken, L., & Gurry, R. W. (1945). The system iron-oxygen. I. The wüstite field and related equilibria. *Journal of the American Chemical Society*, *67*(8), 1398–1412. https://doi.org/10.1021/ja01224a050

Darken, L., & Gurry, R. W. (1946). The system iron—oxygen. II. Equilibrium and thermodynamics of liquid oxide and other phases. *Journal of the American Chemical Society*, *68*(5), 798–816. https://doi.org/10.1021/ja01209a030

Dickson, W. R., & Dismukes, E. B. (1962). The electrolysis of FeO-CaO-SiO2 melts. *Transactions of the Metallurgical Society of AIME*, *224*, 505–511.

Dancy, E. A., & Derge, G. J. (1966). Electrical conductivity of FeOx-CaO slags. *Transactions of the Metallurgical Society of AIME*, *236*, 1642.

Ellingham, H. J. T. (1944). Reducibility of oxides and sulfides in metallurgical processes. *Journal of the Society of Chemical Industry*, *63*, 125–133.

Eugster, H. P. (1957). Heterogeneous reactions involving oxidation and reduction at high pressures and temperatures. *The Journal of Chemical Physics*, *26*(6), 1760–1761. https://doi.org/10.1063/1.1743626

Eugster, H. P. (1959). Reduction and oxidation in metamorphism. In: Abelson, P. H. (ed.) *Researches in Geochemistry*. Volume 1. New York: John Wiley & Sons, pp. 397–426.

Eugster, H. P. (1977). Compositions and thermodynamics of metamorphic solutions. In: Fraser, D. G. (ed.) *Thermodynamics in Geology*. Dordrecht: D. Reidel Publishing Company, pp. 183–202.

Eugster, H. P., & Wones, D. R. (1962). Stability relations of the ferruginous biotite, annite. *Journal of Petrology*, *3*, 82–125. https://doi.org/10.1093/petrology/3.1.82

Feig, S. T., Koepke, J., & Snow, J. E. (2010). Effect of oxygen fugacity and water on phase equilibria of a hydrous tholeiitic basalt. *Contributions to Mineralogy and Petrology*, *160*, 551–568. doi:10.1007/s00410-010-0493-3

Fraser, D. G. (1975). Activities of trace elements in silicate melts. *Geochimica et Cosmochimica Acta*, *39*(11), 1525–1530. https://doi.org/10.1016/0016-7037(75)90154-4

Frost, B. R. (1991). Introduction to oxygen fugacity and its petrologic importance. *Reviews in Mineralogy and Geochemistry*, *25*, 1–9. https://doi.org/10.1515/9781501508684-004

Frost, D. J., & McCammon, C. A. (2008). The redox state of Earth's mantle. *Annual Review of Earth and Planetary Science*, *36*, 389–420. https://doi.org/10.1146/annurev.earth.36.031207.124322

Gaillard, F., Scaillet, B., Pichavant, M., & Iacono-Marziano, G. (2015). The redox geodynamics linking basalts and their mantle sources through space and time. *Chemical Geology*, *418*, 217–233. https://doi.org/10.1016/j.chemgeo.2015.07.030

Giggenbach, W. F. (1980). Geothermal gas equilibria. *Geochimica et cosmochimica Acta*, *44*(12), 2021–2032. https://doi.org/10.1016/0016-7037(80)90200-8

Giggenbach, W. F. (1987). Redox processes governing the chemistry of fumarolic gas discharges from White Island, New Zealand. *Applied Geochemistry*, *2*(2), 143–161. https://doi.org/10.1016/0883-2927(87)90030-8

Gudmundsson, G., & Wood, B. J. (1995). Experimental tests of garnet peridotite oxygen barometry. *Contributions to Mineralogy and Petrology*, *119*(1), 56–67. https://doi.org/10.1007/BF00310717

Hasegawa, M. (2014) Ellingham Diagram. *Treatise on Process Metallurgy*, Volume *3*, 507–513. http://dx.doi.org/10.1016/B978-0-08-096986-2.00032-1

Haskin, L. A., Colson, R. O., Lindstrom, D. J., Lewis, R. H., & Semkow, K. W. (1992, September). Electrolytic smelting of lunar rock for oxygen, iron, and silicon. In: Nasa. Johnson Space Center. The Second Conference on Lunar Bases and Space Activities of the 21st Century, Volume 2, 411–422.

Hillert, M., Jansson, B. O., & Sundman, B. O. (1985). A two-sublattice model for molten solutions with different tendency for ionization. *Metallurgical Transactions A*, *16*(1), 261–266. https://doi.org/10.1007/BF02816052

Kress, V. C., & Carmichael, I. S. (1991). The compressibility of silicate liquids containing Fe_2O_3 and the effect of composition, temperature, oxygen fugacity and pressure on their redox states. *Contributions to Mineralogy and Petrology*, *108*(1–2), 82–92. https://doi.org/10.1007/BF00307328

Lavoisier A. (1777) Mémoire sur la combustion en général, Académie des sciences, Mémoires de l'Académie Royale, Paris, 592–600.

Le Losq, C., Moretti, R., Oppenheimer, C., & Neuville, D. R. (2020) In situ XANES study of the influence of varying temperature and oxygen fugacity on iron oxidation state and coordination in a phonolitic melt. *Contributions to Mineralogy and Petrology*, *175*, 64–77. doi: 10.1007/s00410-020-01701-4

Lewis, G. N., & Randall, M. (1961). *Thermodynamics*, 2nd Edition. Revised By Kenneth Pitzer and Leo Brewer. McGraw-Hill Book Company. 723pp.

Ripley, E. M., & Li, C. (2013). Sulfide saturation in mafic magmas: Is external sulfur required for magmatic Ni-Cu-(PGE) ore genesis? *Economic Geology*, *108*(1), 45–58. https://doi.org/10.2113/econgeo.108.1.45

Littlewood, R. (1962). Diagrammatic representation of the thermodynamics of metal-fused chloride systems. *Journal of the Electrochemical Society*, *109*, 525–534.

Magnien, V., Neuville, D. R., Cormier, L., Roux, J., Hazemann, J-L., Pinet, O., and Richet, P. (2006). Kinetics of iron redox reactions in silicate liquids: a high-temperature X-ray absorption and Raman spectroscopy study. *Journal of Nuclear Materials*, *352*, 190–195. https://doi.org/10.1016/j.jnucmat.2006.02.053

Magnien, V., Neuville, D. R., Cormier, L., Roux, J., Hazemann, J-L., de Ligny D., et al. (2008). Kinetics and mechanisms of iron redox reactions in silicate melts: The effects of temperature and alkali cations. *Geochimica et Cosmochimica Acta*, *72*, 2157–2168. https://doi.org/10.1016/j.gca.2008.02.007

Mallmann, G., & O'Neill, H. S. C. (2009). The crystal/melt partitioning of V during mantle melting as a function of oxygen fugacity compared with some other elements (Al, P, Ca, Sc, Ti, Cr, Fe, Ga, Y, Zr and Nb). *Journal of Petrology*, *50*(9), 1765–1794. doi:10.1093/petrology/egp053

Mao, H., Hillert, M., Selleby, M., & Sundman, B. (2006). Thermodynamic assessment of the $CaO–Al_2O_3–SiO_2$ system. *Journal of the American Ceramic Society*, *89*(1), 298–308. https://doi.org/10.1111/j.1551-2916.2005.00698.x

Mattioli, G. S., & Wood, B. J. (1988). Magnetite activities across the $MgAl_2O_4$-Fe_3O_4 spinel join, with application to thermobarometric estimates of upper mantle oxygen fugacity. *Contributions to Mineralogy and Petrology*, *98*(2), 148–162. https://doi.org/10.1007/BF00402108

Moretti, R. (2005). Polymerisation, basicity, oxidation state and their role in ionic modelling of silicate melts. *Annals of Geophysics*, *48*, 4/5, 583–608. https://doi.org/10.4401/ag-3221

Moretti, R. (2021). Ionic syntax and equilibrium approach to redox exchanges in melts: basic concepts and the case of iron and sulfur in degassing magmas. In: Moretti, R., and Neuville, D. R. (eds.) *Redox Magma Geochemistry. Geophysical Monograph Series 266*. American Geophysical Union.

Moretti, R., & Baker, D. R. (2008). Modeling of the interplay of fO2 and fS2 along the FeS-Silicate Melt equilibrium. *Chemical Geology*, *256*, 286–298. doi:10.1016/j.chemgeo.2008.06.055.

Moretti, R., & Ottonello, G. (2003). Polymerization and disproportionation of iron and sulfur in silicate melts: insights from an optical basicity-based approach. *Journal of Non-Crystalline Solids*, *323*, 111–119. https://doi.org/10.1016/S0022-3093(03)00297-7

Moretti, R., Arienzo, I., Civetta, L., Orsi, G., & Papale, P. (2013) Multiple magma degassing sources at an explosive volcano. *Earth and Planetary Sciences Letters*, *367*, 95–104. https://doi.org/10.1016/j.epsl.2013.02.013

Moretti, R., & Stefánsson, A. (2020). Volcanic and geothermal redox engines. *Elements: An International Magazine of Mineralogy, Geochemistry, and Petrology*, *16*(3), 179–184. https://doi.org/10.2138/gselements.16.3.179

Nadoll, P., Angerer, T., Mauk, J.L., French, D., & Walshe, J. (2014). The chemistry of hydrothermal magnetite: A review. *Ore Geology Reviews*, *61*, 1–32. https://doi.org/10.1016/j.oregeorev.2013.12.013

Nash, W. M., Smythe, D. J., & Wood, B. J. (2019). Compositional and temperature effects on sulfur speciation and solubility in silicate melts. *Earth and Planetary Science Letters*, *507*, 187–198. https://doi.org/10.1016/j.epsl.2018.12.006

Neuville, D. R., Cicconi, M. R., & Le Losq, C. (2021). How to measure the oxidation state of multivalent elements in minerals, glasses and melts? In: Moretti, R., and Neuville, D. R. *Magma Redox Geochemistry*. Geophysical Monograph Series 266. American Geophysical Union.

Ottonello, G. (1997). *Principles of Geochemistry*. Columbia University Press, 894 pp.

Ottonello, G., & Moretti, R. (2004). Lux-Flood basicity of binary silicate melts. *Journal of Physics and Chemistry of Solids*, *65* (8–9), 1609–1614. https://doi.org/10.1016/j.jpcs.2004.01.012

Ottonello, G., Moretti, R., Marini, L., & Zuccolini, M. V. (2001). Oxidation state of iron in silicate glasses and melts: a thermochemical model. *Chemical Geology*, *174*(1–3), 157–179. https://doi.org/10.1016/S0009-2541(00)00314-4

Pichavant, M., Costa, F., Burgisser, A., Scaillet, B., Martel, C., & Poussineau, S. (2007). Equilibration scales in silicic to intermediate magmas—implications for experimental studies. *Journal of Petrology*, *48*(10), 1955–1972. https://doi.org/10.1093/petrology/egm045

Pinet, O., Phalippou, J., & Di Nardo, C. (2006). Modeling the redox equilibrium of the Ce^{4+}/Ce^{3+} couple in silicate glass by voltammetry. *Journal of Non-Crystalline Solids*, *352*(50–51), 5382–5390. https://doi.org/10.1016/j.jnoncrysol.2006.08.034

Raymond, J., Williams-Jones, A. E., & Clark, J. R. (2005). Mineralization associated with scale and altered rock and pipe fragments from the Berlın geothermal field, El Salvador; implications for metal transport in natural systems. *Journal of Volcanology and Geothermal Research*, *145*, 81–96. doi:10.1016/j.jvolgeores.2005.01.003

Schreiber, H. D. (1987). An electrochemical series of redox couples in silicate melts: a review and applications to geochemistry. *Journal of Geophysical Research: Solid Earth*, *92*(B9), 9225–9232. https://doi.org/10.1029/JB092iB09p09225

Sokhanvaran, S., Lee, S.-K., Lambotte, G., & Allanore, A. (2016). Electrochemistry of molten sulfides: Copper extraction from BaS-Cu_2S. *Journal of The Electrochemical Society*, *163*, D115–D120.

Semkow, K. W., & Haskin, L. A. (1985). Concentrations and behavior of oxygen and oxide ion in melts of composition $CaO{\cdot}MgO{\cdot}xSiO_2$. *Geochimica et Cosmochimica Acta*, *49*(9), 1897–1908. https://doi.org/10.1016/0016-7037(85)90084-5

Toop, G. W., & Samis, C. S. (1962a). Some new ionic concepts of silicate slags. *Canadian Metallurgical Quarterly*, *1*, 129–152. https://doi.org/10.1179/cmq.1962.1.2.129

Toop, G. W., & Samis, C. S. (1962b). Activities of ions in silicate melts. *Transactions of the Metallurgical Society of AIME*, *224*, 878–887.

Trémillon B. (1974). *Chemistry in non-aqueous solvents*. Dordrecht: D. Reidel Publishing Company. 285 pp.

Vaughan, D. J. (2005). Minerals/Sulphides. *Encyclopedia of Geology. Elsevier.* 574–586.

Zhang, J., Matsuura, H., & Tsukihashi, F. (2014). Processes for Recycling. *Treatise on Process Metallurgy*, Volume *3*, 1507–1561. http://dx.doi.org/10.1016/B978-0-08-096988-6.00036-5